ACS OMEGA

Article

Cite This: ACS Omega XXXX, XXX, XXX−XXX

http://pubs.acs.org/journal/acsodf

Hydrodynamic Determination of the Kinematic Viscosity of Waste Brines

Martí Sánchez-Juny,*[,†] Arnau Triadú,[‡] Antoni Andreu,[§] and Ernest Bladé[†]

[†]Barcelona School of Civil Engineering, Universitat Politècnica de Catalunya BarcelonaTECH, Jordi Girona 1-3, Building D1, 08034 Barcelona, Spain

[‡]Environmental Department, Baix Penedès County Council, 43700 El Vendrell, Spain

[§]Civil Engineering Department, Company Aigües de Barcelona, 08038 Barcelona, Spain

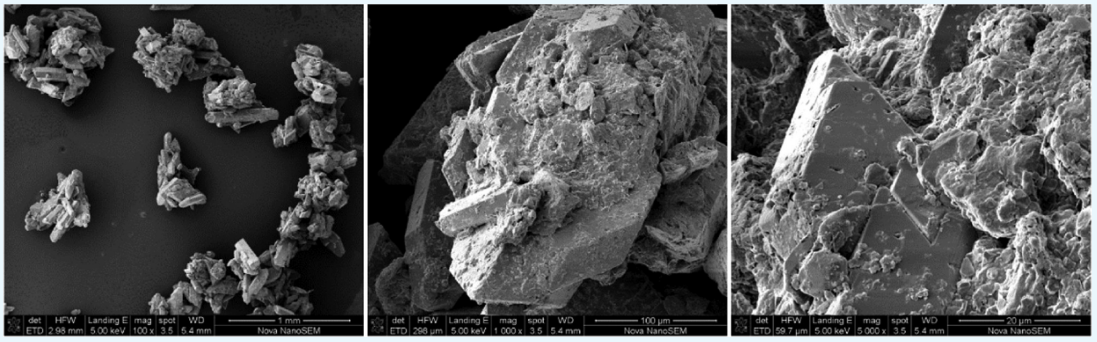

ABSTRACT: Wastewater from a potash mine in the central region of Catalonia is transported by means of a collector that runs more than 100 km, spilling into the sea on the Catalan central coast. To analyze the hydraulics of this infrastructure, the values of the basic parameters that condition the flow, such as the absolute roughness of poly(vinyl chloride) (PVC) pipes and the viscosity of the transported brine mixtures, must be characterized. There exists uncertainty about the value of absolute roughness of a PVC pipe as described in the literature; nevertheless, if the pipe is smooth, the influence of the absolute roughness in the hydraulic determination of viscosity will not be significant. In this work, an experimental procedure based on a hydraulic analysis was applied to estimate the kinematic viscosity of a brine mixture, depending on its temperature and concentrations of salts and fines. The results obtained were compared with the results from experiments using an Ostwald viscometer.

INTRODUCTION

The present experimental work is part of a study whose main objective was to analyze the hydraulic behavior of a pipeline when transporting the waste brine generated in the salt mines of the Bages region in Catalonia (Spain) (Figure 1) before it is spilled into the Mediterranean Sea. In Spain, at the moment, there are no local regulations about permitted salt concentrations before spilling into the sea. Despite the high salt concentration of the transported waste brines, these are lower than spilled waste from other processes such as a desalination water process. It can be noticed that Spain is one of the world's leading producers of desalinated water, whose waste is fundamentally spilled into the sea through a marine outfall. Apart from the several different saline compounds that constitute this salt, it also contains a small percentage of insoluble fine particles. Prior to resorting to a hydraulic analysis, it was necessary to determine the viscosity of the fluid. For this purpose, a simple hydraulic experimental model was designed and constructed in the Fluid Mechanics Laboratory of the Civil Engineering School of UPC-BarcelonaTECH. There, the value of the brine viscosity was obtained indirectly for different concentration values of the solid part. An Ostwald viscometer was also used to calculate the viscosity of the same brine samples, after first filtering off the fines, to know the effect of the insoluble particles on the viscosity of these samples.

Consequently, the scope of this paper is:

- To calibrate the absolute roughness of a PVC pipeline of an experimental facility in the laboratory.
- To estimate the viscosity of highly concentrated brine, depending on the concentration of solute and its temperature.
- To analyze the effect of insoluble fine particles on brine viscosity.

It is well known how the viscosity of water varies depending on the fluid temperature. In the case of brine dissolution, this viscosity additionally also varies depending on the concentration of solute. Several authors[1−3] have studied how water viscosity varies when a particular soluble compound, such as sodium chloride or potassium chloride, is added. As could be

Received: July 13, 2019
Accepted: October 30, 2019

DOI: 10.1021/acsomega.9b02164
ACS Omega XXXX, XXX, XXX−XXX

Figure 1. Schematic layout of the pipeline to transport waste brines generated in the salt mines in the Bages region in Catalonia. Free domain images.

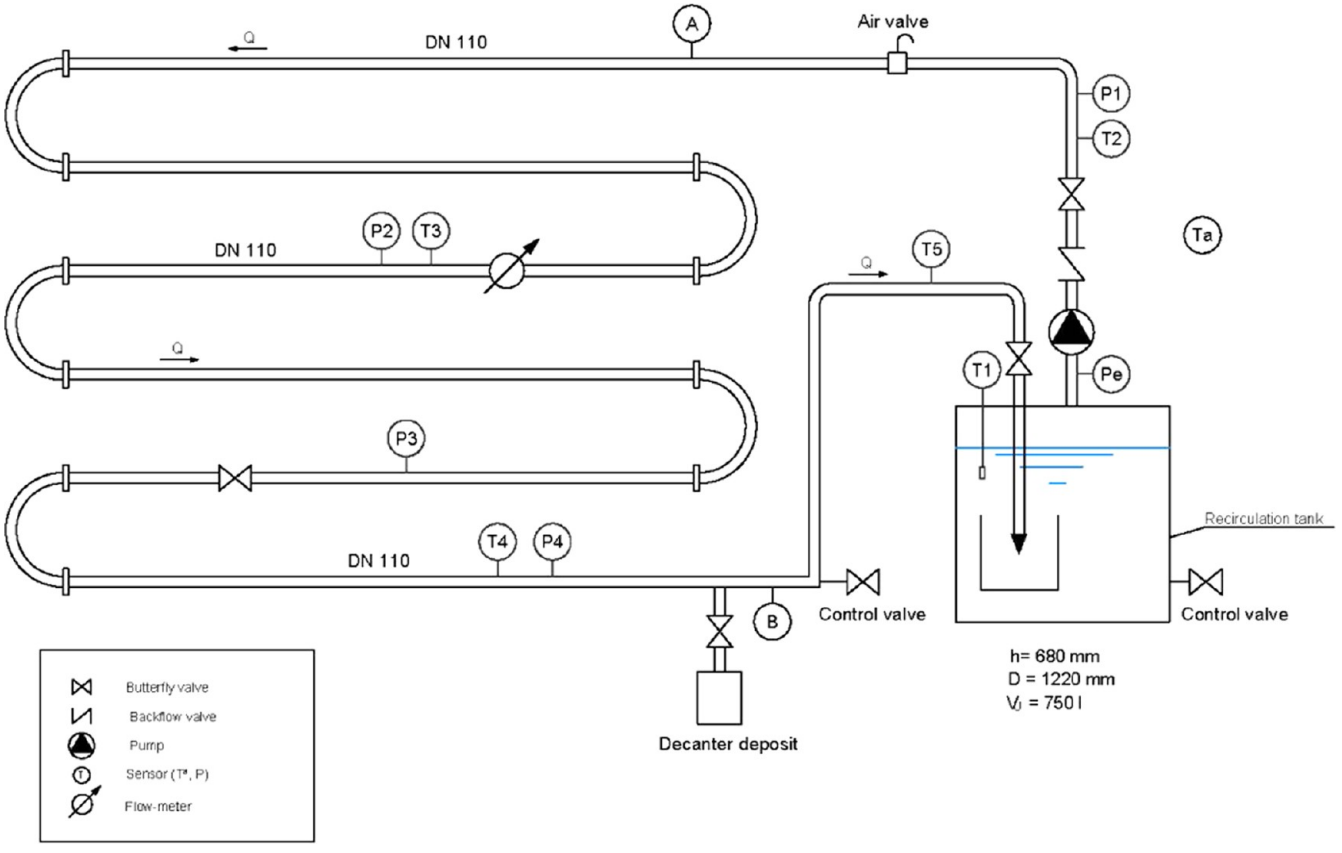

Figure 2. Schematic layout of the experimental facility (EF).

expected, the higher the salt concentration, the higher the viscosity of the solution. Kestin et al.[4] presented the viscosity values of sodium chloride solutions depending on the temperature (for a range between 20 and 150 °C) and on the concentration of solute (for a range between 0 and 6 mol/kg). Gonçalves and Kestin[5] presented the viscosity of

DOI: 10.1021/acsomega.9b02164
ACS Omega XXXX, XXX, XXX−XXX

potassium chloride solutions for temperatures between 25 and 50 °C and solute concentrations of up to 4.55 mol/kg. Finally, Phang and Stokes[6] made the same analysis for solutions of magnesium chloride, at 25 °C and for concentrations between 0 and 6 mol/kg.

The present study deals with a salt solution formed mainly by NaCl but also containing KCl, $MgCl_2$, and $CaSO_4$ among other compounds. The viscosity of the mixture constituted of this salt varies according to its interaction with these compounds. For example, in the case of NaCl and KCl solutions, Zhang and Han[7] presented the viscosity at 25 °C for different molar ratios in the two solutes and for concentrations between 0 and 6 mol/kg. Similarly, Qiblawey and Abu-Jdayil[8] provided the viscosity for solutions formed by NaCl and $MgCl_2$ between 25 and 45 °C for different molar ratios and solute concentrations between 0 and 4 mol/kg.

In addition to the interaction between different solutes, it should be considered that the presence of insoluble solid particles in the brine mixture also modifies its viscosity. According to Gillies et al.,[9] when a mixture contains insoluble material in the form of fines it is necessary to measure its viscosity experimentally. However, several equations for calculating viscosity can be found in the literature.[10−14] Nevertheless, as all the correlations presented in the literature for the calculation of the viscosity of sediment mixtures are designed for particles of the same diameter, it is necessary to measure the viscosity[9] experimentally for real cases involving mixtures with heterogeneous grain sizes.

MATERIALS AND METHODS

Experimental Setup. The experimental facility (EF) was built in the Fluid Mechanics Laboratory of the Civil Engineering School of UPC-BarcelonaTECH.

Table 1. Density, Solid Mass Percentage, and Solid Concentration of Different Mixtures Tested in the EF[a]

brine mixture	density (kg/m^3)	solid mass % (solids kg/mixture kg)	solids concentration (kg/m^3)
A	1157.5	22.2	258
B	1141.6	20.0	229
C	1134.1	19.2	217
D	1124.1	18.5	209
E	1109.3	16.9	187
F	1201.6	27.5	331
G	1197.6	27.2	326
H	1160.4	22.5	261

[a]The word "solid" refers to all of the solid particles, whether soluble or not.

The schematic layout of the pipeline system used in this study is shown in Figure 2. This facility consisted of a closed PVC loop of length 71 m, made of high-density polyethylene (HDPE) pipes. The setup was composed of a 100 mm inner diameter pipeline connected to a 1.1 kW centrifugal pump (company HASA, model RGM-S-17/2). A paddle wheel flow meter (Sensotec, model VTH100) was installed for continuous monitoring of the flow rate, as shown in Figure 2. The velocity measurement interval was from 0 to 6 m/s, and its uncertainty was ±0.03 m/s. The pressure drop was measured at five points using piezoresistive transducers (Messtech, model FR-401): at the inlet (P_e), at the outlet (P1) of the pump, and at three more points distributed along the pipeline (P2−P4). Sensors

Table 2. Mass Percentage of the Different Ions Present in a Sample of Salt from the Mine in Bages Region[15]

compound	mass %
sodium (% Na)	35.7
calcium (% Ca)	0.60
magnesium (% Mg)	0.24
strontium (% Sr)	traces
potassium (% K)	1.2
bicarbonate (% HCO_3^-)	traces
chloride (% Cl^-)	57.6
sulfate (% SO_4^{2-})	2.7
bromide (% Br^-)	traces
insoluble	1.14

Table 3. Mass Percentage of the Different Compounds or Insoluble Elements Present in a Sample of Salt from the Mine in Bages Region[15]

component	mass %
NaCl (%)	91.49
$CaSO_4$ (%)	3.30
KCl (%)	2.30
$MgCl_2$ (%)	0.95
insolubles (%)	1.14

P1−P4 measured relative pressures from 0 to 1.5 bar, while P_e measured pressures within a range from −1 bar to 0. The slurry mixture was prepared in a cylindrical aluminum tank (Hackman Wedholms) that acts as an accumulator deposit. The capacity of this tank was 0.750 m^3, and it had an inner diameter of 1.22 m. The temperature of the flow was also recorded by RTD sensors (Desin, model PT100) at five points: one inside the accumulator deposit (T1), three along the pipeline loop (T2−T4), and the last one in the pipe returning to the deposit (T5). Their tolerance was ±0.03 °C at 0 °C and ±0.08 °C at 100 °C. All five RTDs were calibrated, and the maximum deviation between them was lower than 0.3 °C.

The EF loop presented some non-negligible local energy losses, which complicated its setup and later the hydraulic analysis.

All pressure transducers are connected to the pipe by means of a threaded element from which there is a spit that allows to extract fluid from inside the pipe. Likewise, close to the recirculation tank, there is also a small decanter deposit from which, once the system is stopped, a sediment sample can be collected.

Properties of the Tested Brines. The EF described above allows recirculation of a solution of water and salt. Salt from the mines of the Bages region was used to produce the brine or slurry mixtures tested in this study. The characteristics of the brines (density, solid mass percentage, and solid concentration) are shown in Table 1. To ensure maximum dissolution of the salt in water, the mixture was circulated for at least an hour through the experimental loop. Subsequently, the density and solid concentration of the mixture were measured for a sample extracted from the flow. The chemical composition of the tested brine is shown in Table 2, and it is obtained through inductively coupled plasma optical emission spectroscopy (ICP-OES) and ionic chromatography:[15]

DOI: 10.1021/acsomega.9b02164
ACS Omega XXXX, XXX, XXX−XXX

Figure 3. Head of the pressure transducer (left) and its point of connection to the pipeline (right), both after some hours in contact with the brine flow. Photographs courtesy of Arnau Triadú. Copyright 2017. Free domain images.

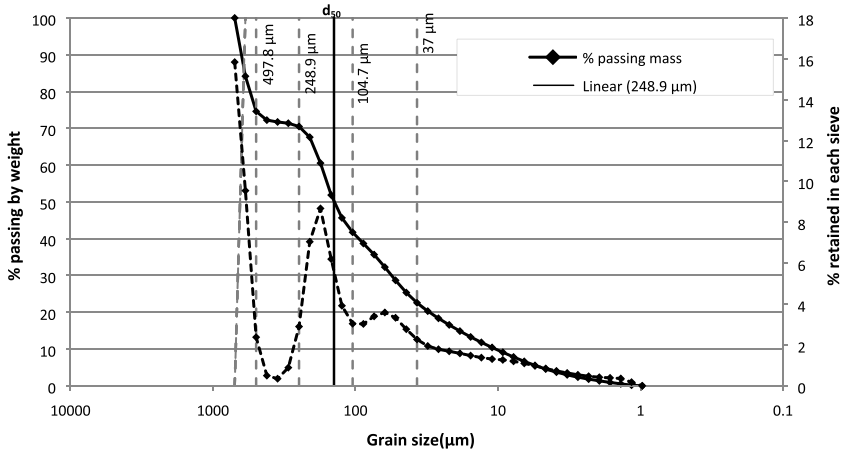

Figure 4. Graphs (in %) of passing (solid line) and retained (dashed line) material versus sieve size. The d_{50} grain size is 141.5 μm.

The salt mines of Bages region in Catalonia have been exploited since 1912 for the extraction of potash. The total composition of the salt extracted is well known;[16−18] therefore, for calculating the moles of each element in 100 g of sample, it is considered that the cations of sodium, magnesium, and potassium form chlorides and calcium forms sulfates. This is not an exact calculation but provides an approximate idea of the percentage in weight of each compound in the tested brine (Table 3). Apart from the several compounds determined in this way, there is also a non-negligible insoluble part made up specifically of fines (clay and silt).

The insoluble part was accurately analyzed from a sample obtained from the connections of the pressure transducers to the pipeline (Figure 3).

The granulometric analysis of the same sediment sample is shown in Figure 4. The granulometric curve (solid line) shows a heterogeneous material, as it contains several dominant particle sizes. This can also be observed in the dashed curve, which represents the percentage in weight of particles that are retained by each sieve; the presence of several peaks denotes that there are some particle sizes that are more common than others. The particle size with a higher presence in the sediment sample corresponds to the maximum of this curve, which is between 498 and 704 μm and represents 25.4% of the total. Regarding the two peaks of the dashed curve, it can be appreciated that 28.75% of the particles are accumulated between the sieves of 105 and 249 μm, while 19.16% are retained between the sieves of 37 and 105 μm. Finally, there are non-negligible 22.58% of the particles below 37 μm. The figure summarizes these data and shows an interval with almost no particles between sieves from 249 to 498 μm.

The figure also shows that the diameter corresponding to 50% of the accumulated distribution (d_{50}) is 141.5 μm. This d_{50} is usually used as a particle size representative of a sample of sediments, but in the case of a distribution of heterogeneous sizes, as in our case, this representability decreases.

Finally, the analysis of the sample shows that the maximum concentration of solids (that is, the different dissolved salts plus the suspended particles) that the mixture is capable of transporting is 331 kg/m^3. The verification consisted simply of adding enough brine to the filled tank to saturate it and removing the mixture to favor the dissolution of the soluble elements. Brine was added until a deep sediment bed of a few centimeter thickness was formed at the bottom of the tank. Then, this mixture was circulated for more than an hour to allow it to reach equilibrium with regard to the dissolution−

DOI: 10.1021/acsomega.9b02164
ACS Omega XXXX, XXX, XXX−XXX

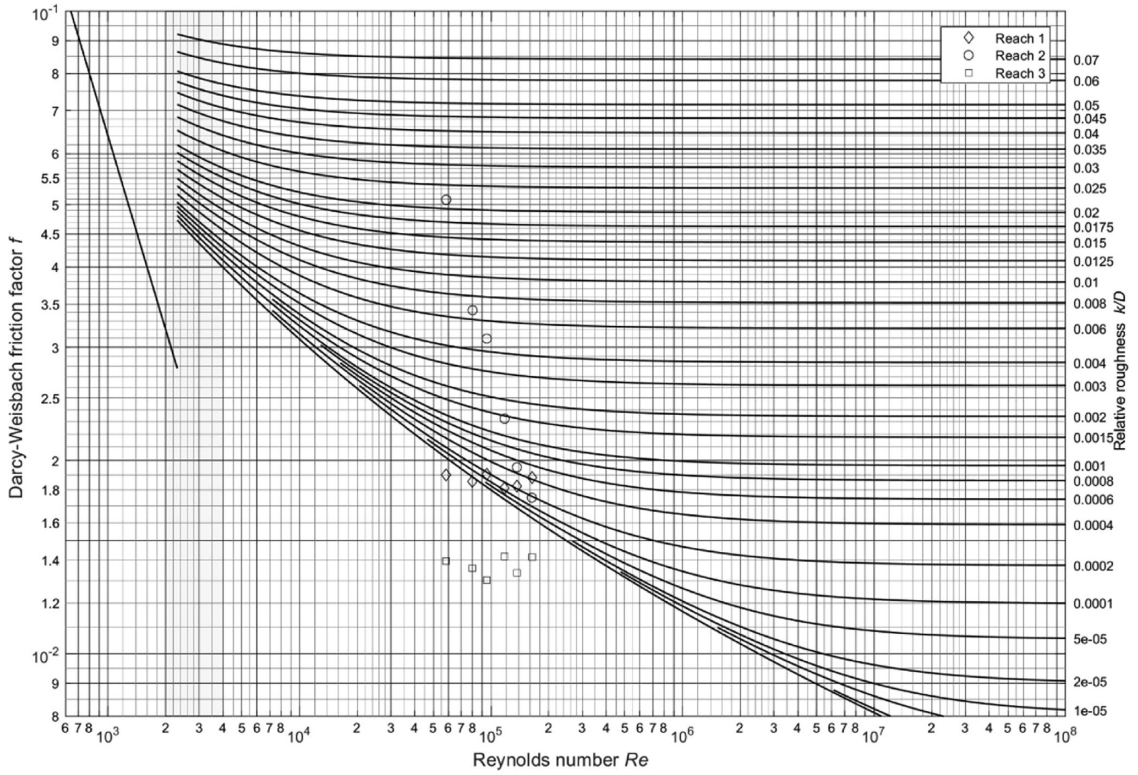

Figure 5. Friction coefficient values obtained for each of the three controlled sections of the EF, from the experiments with clear water, as reflected in Moody's diagram. Preliminary results with local head losses obtained from the literature.

precipitation of salts and the drag−sedimentation of insoluble particles. Afterward, a sample of the flowing mixture was taken and its density and concentration were measured. The resulting values were 1202 kg/m^3 and an equivalent solid percentage of 27.5% (kg of total solids/kg of mixture), respectively. Finally, to ensure that the measured concentration was the actual saturation of the mixture, more brine was added to the mixture and the process repeated, until it was observed that the same result was obtained.

Experimental Methodology. The main aim of the experimental procedure was to obtain the viscosity of the different brines tested. Different experimental campaigns were carried out for the purpose to determine the viscosity and EF parameters: local head losses and absolute roughness. The process followed for the determination of viscosity was as follows:

1. Determination of the local head losses due to the elbows and the butterfly valve located in the experimental loop. To this end, experiments with clear water were carried out for six different flow rates. The local energy losses in each of the three controlled sections in the EF were calibrated independently by means of tests with clear water using the equation

$$h_{loc} = K \cdot \frac{v^2}{2g} + \Delta h \quad (1)$$

where h_{loc} represents the local head losses, v is the average velocity, g is the gravity acceleration, K is a dimensionless local head loss coefficient, and Δh is a fitting parameter. The process to calibrate the values of K and Δh is explained in next section.

2. Determination of the absolute roughness of the pipe from the same experiments with clear water.
3. Estimation of the friction factors (f) for all flow rates and brine concentrations. This process was performed independently for each test and for each of the three reaches of the EF controlled by sensors. From the values of the hydraulic gradient, the friction coefficient for each test and reach was obtained using the Darcy−Weisbach equation.
4. Determination of the viscosity of the brines. Viscosity of the brine mixtures used in the tests was determined by fitting a nonlinear regression to the points of observed pressure values using the Darcy−Weisbach relation and the Swamee and Jain equation. The observed pressure gradients correspond to the entire EF loop, from sensors P1−P4 (Figure 1). Since the value of the absolute roughness of the pipe is already known, the only remaining unknown parameter in the previous equations is the viscosity of the brine mixture.

As is well known, the viscosity of a fluid depends on its temperature. That is why all of the tests were carried out in a controlled environment, with a temperature close to 25 °C.

RESULTS AND DISCUSSION

Local Energy Losses in the EF. The calibration of the parameters K and Δh of the local head losses, eq 1), was done in three steps.

In the first step, only the contribution of K to the total head losses, h_{loc}, was considered (Δh was set to zero). K was estimated using the tables provided by Lencastre.[19] From the observed energy losses, and using the Darcy−Weisbach equation for the evaluation of the friction losses, a friction factor (f) was obtained for each flow rate. Figure 5 shows the

DOI: 10.1021/acsomega.9b02164
ACS Omega XXXX, XXX, XXX−XXX

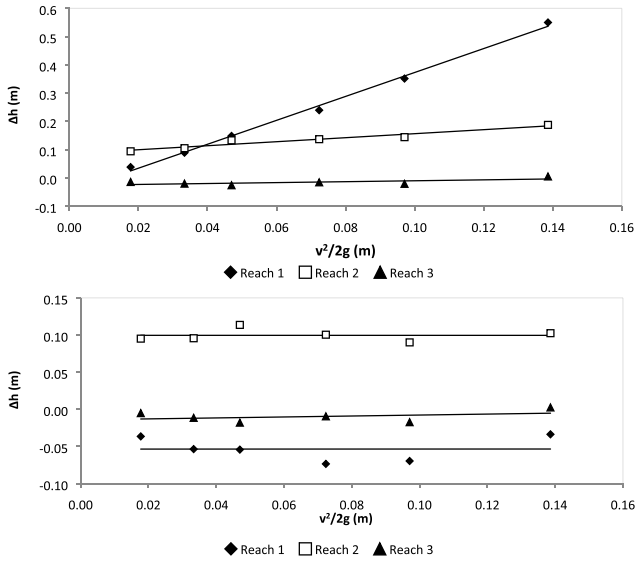

Figure 6. Δh values obtained for the first iteration (above) and the third one (below), during the calibration of local head losses for each monitored section of the EF, depending on $v^2/2g$.

Table 4. Final Values of K and Δh, Equation 1), and Its Standard Deviation Obtained at the Final Iteration To Calibrate the Local Energy Losses in Each One of the Three Monitored Sections in EF

reach	K	σ_k	Δh	$\sigma_{\Delta h}$
1	4.787	0.002	−0.054	0.016
2	1.144	0.002	0.100	0.008
3	0.515	0.001	−0.010	0.008

results of this first estimation of Darcy−Weisbach friction factors. As can be clearly observed, they do not follow a particular relative roughness curve. Since all of the tests were carried out under the same conditions and in the same loop, the relative roughness values obtained in each test should be the same, whereas they were substantially different.

In the second step, the friction factor was estimated through the Nikuradse[20] expression. Considering that the pipe used in the EF was made of PVC, and also the range of the Reynolds numbers, the flow conditions are of smooth turbulent flow, and for that reason, the Nikuradse[20] expression in which the friction factor is a function of the Reynolds number but not of the relative roughness is appropriate. In this second step, eq 1) was used to evaluate the local head losses, with the same values of K as in the previous step. The parameter adjusted to fit the numerical results of total energy losses with the observed ones was Δh. From this adjustment, it was seen that numerical results could not fit with the observed ones if a constant value of Δh was used. Figure 6a shows the linear relation between Δh and the kinetic energy per unit of weight in each test and each reach of the EF in this second step. This linear variation shows that Δh can be decomposed in a term dependent on $v^2/2g$ and a constant term (which will be the new Δh for the third step). In the third step, the linear variation of the local losses was added to the K coefficient, thus resulting in a new value of K, whereas Δh was maintained constant for each reach (Figure 6b). The final results of constant K and Δh in each controlled reach of the loop are shown in Table 4. Negative values of Δh can appear, as no physical meaning is associated with this parameter, although it has a function of compensating possible errors or deviations in the experimental procedure.

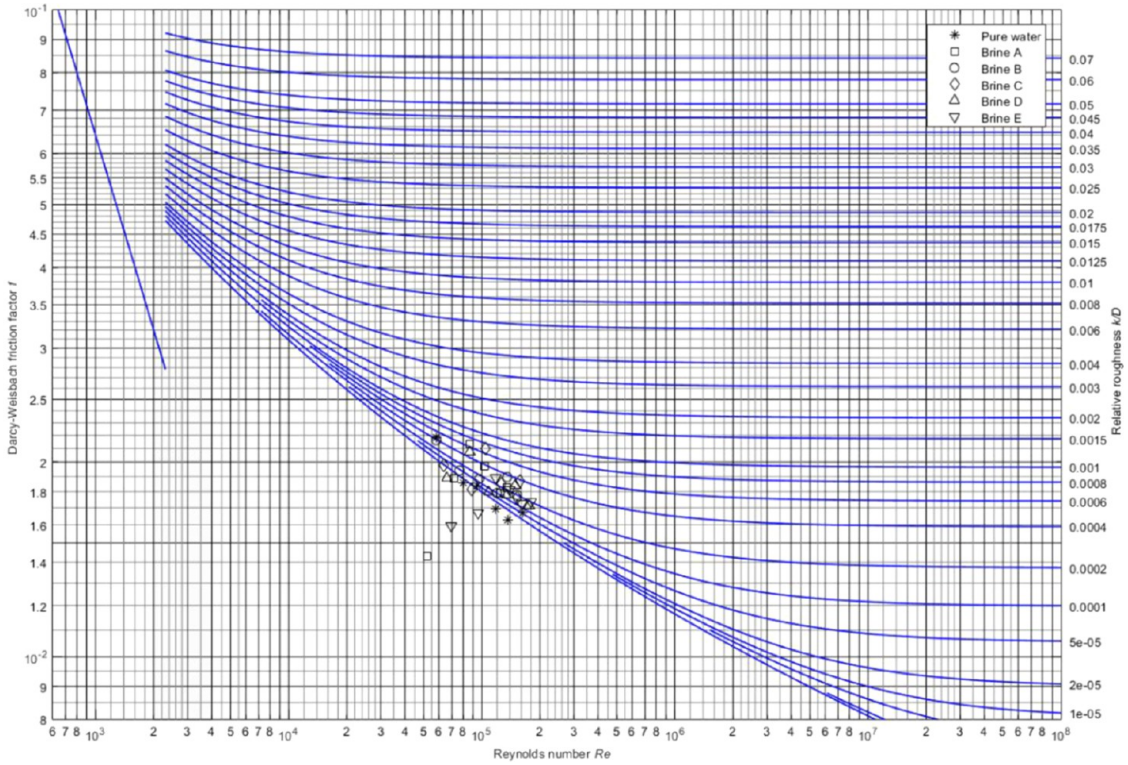

Figure 7. Friction coefficient values obtained for each of the three reaches of the EF, from the experiments with clear water. Results were obtained after the calibration of localized head losses.

DOI: 10.1021/acsomega.9b02164
ACS Omega XXXX, XXX, XXX−XXX

Table 5. Hydraulic Gradient (S_f) and Darcy–Weisbach Friction Factor (f) Obtained from Experimental Data, for Each Test and Reach in the EF[a]

		S_f (mcm/m)				f			
test	Reynolds number	reach 1	reach 2	reach 3	average	reach 1	reach 2	reach 3	total
H_2O 01	1.63×10^5	0.0234	0.0228	0.0264	0.0242	0.0168	0.0163	0.0169	0.0167
H_2O 02	1.36×10^5	0.0158	0.0159	0.0190	0.0169	0.0164	0.0163	0.0162	0.0163
H_2O 03	1.18×10^5	0.0120	0.0127	0.0156	0.0134	0.0163	0.0178	0.0176	0.0169
H_2O 04	9.50×10^4	0.0085	0.0095	0.0112	0.0097	0.0184	0.0200	0.0175	0.0184
H_2O 05	8.00×10^4	0.0062	0.0064	0.0093	0.0073	0.0190	0.0194	0.0185	0.0186
H_2O 06	5.84×10^4	0.0041	0.0031	0.0068	0.0047	0.0223	0.0174	0.0199	0.0218
BRI_A 01	1.35×10^5	0.0226	0.0184	0.0264	0.0224	0.0190	0.0155	0.0197	0.0182
BRI_A 02	1.25×10^5	0.0190	0.0151	0.0231	0.0191	0.0185	0.0148	0.0197	0.0179
BRI_A 03	1.03×10^5	0.0149	0.0109	0.0173	0.0143	0.0215	0.0155	0.0208	0.0197
BRI_A 04	8.68×10^4	0.0121	0.0071	0.0137	0.0110	0.0248	0.0142	0.0216	0.0213
BRI_A 05	7.21×10^4	0.0072	0.0039	0.0103	0.0071	0.0214	0.0115	0.0213	0.0189
BRI_A 06	5.18×10^4	0.0023	0.0008	0.0074	0.0035	0.0136	0.0042	0.0289	0.0143
BRI_B 01	1.52×10^5	0.0227	0.0186	0.0257	0.0223	0.0187	0.0152	0.0185	0.0178
BRI_B 02	1.35×10^5	0.0196	0.0149	0.0222	0.0189	0.0203	0.0156	0.0199	0.0190
BRI_B 03	1.20×10^5	0.0140	0.0105	0.0183	0.0143	0.0187	0.0142	0.0204	0.0179
BRI_B 04	9.70×10^4	0.0101	0.0068	0.0133	0.0101	0.0204	0.0138	0.0207	0.0188
BRI_B 05	7.66×10^4	0.0069	0.0032	0.0097	0.0066	0.0220	0.0096	0.0236	0.0194
BRI_B 06	5.82×10^4	0.0052	0.0012	0.0072	0.0045	0.0276	0.0064	0.0243	0.0216
BRI_C 01	1.57×10^5	0.0217	0.0159	0.0246	0.0207	0.0200	0.0148	0.0200	0.0187
BRI_C 02	1.52×10^5	0.0189	0.0141	0.0229	0.0187	0.0185	0.0139	0.0194	0.0176
BRI_C 03	1.27×10^5	0.0143	0.0097	0.0171	0.0137	0.0201	0.0135	0.0200	0.0185
BRI_C 04	1.05×10^5	0.0117	0.0065	0.0137	0.0106	0.0243	0.0132	0.0221	0.0210
BRI_C 05	8.87×10^4	0.0072	0.0030	0.0101	0.0068	0.0210	0.0084	0.0210	0.0181
BRI_C 06	6.37×10^4	0.0050	0.0004	0.0077	0.0041	0.0279	0.0037	0.0247	0.0198
BRI_D 01	1.76×10^5	0.0233	0.0182	0.0269	0.0228	0.0180	0.0142	0.0183	0.0171
BRI_D 02	1.49×10^5	0.0180	0.0137	0.0221	0.0179	0.0191	0.0147	0.0207	0.0184
BRI_D 03	1.34×10^5	0.0147	0.0102	0.0179	0.0143	0.0192	0.0134	0.0197	0.0178
BRI_D 04	1.09×10^5	0.0096	0.0068	0.0126	0.0097	0.0196	0.0133	0.0197	0.0180
BRI_D 05	8.66×10^4	0.0078	0.0034	0.0104	0.0072	0.0239	0.0104	0.0240	0.0208
BRI_D 06	6.60×10^4	0.0043	0.0009	0.0071	0.0041	0.0231	0.0051	0.0222	0.0189
BRI_E 01	1.80×10^5	0.0225	0.0182	0.0262	0.0223	0.0181	0.0146	0.0188	0.0173
BRI_E 02	1.61×10^5	0.0184	0.0137	0.0217	0.0179	0.0184	0.0137	0.0187	0.0173
BRI_E 03	1.39×10^5	0.0145	0.0104	0.0182	0.0144	0.0193	0.0139	0.0204	0.0181
BRI_E 04	1.18×10^5	0.0112	0.0072	0.0141	0.0108	0.0211	0.0134	0.0206	0.0189
BRI_E 05	9.57×10^4	0.0063	0.0034	0.0104	0.0067	0.0177	0.0101	0.0210	0.0167
BRI_E 06	6.96×10^4	0.0032	0.0012	0.0072	0.0039	0.0175	0.0059	0.0211	0.0159

[a]The average of S_f and f related to the whole loop are also included.

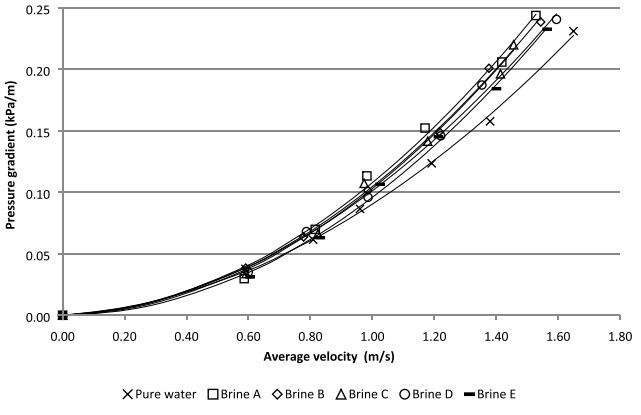

Figure 8. Pressure gradient in the EF (sensors P1–P4 of Figure 2) versus average velocity of each test for all of the tested brine mixtures. Curves were fitted using the Darcy–Weisbach relation.

Table 6. Kinematic Viscosity Obtained for Each One of the Tested Brine Mixtures in the EF at Approximately 25 °C

brine mixture	kinematic viscosity (m^2/s)	variation coefficient for a 95% confidence interval (%)
A	1.13×10^{-6}	10.6
B	1.02×10^{-6}	11.8
C	9.29×10^{-7}	12.9
D	9.08×10^{-7}	13.2
E	8.70×10^{-7}	13.8

Finally, using the estimated constant values of K and Δh of the third step, the friction coefficients required to fit the observed and calculated total energy losses were obtained. These new Darcy–Weisbach friction factors fit better with the smooth turbulent flow zone in Moody's diagram (Figure 7). The values of f for lower Reynolds numbers were the ones that presented greater deviations. This is in agreement with the sensitivity analysis of the friction factor calculation.

DOI: 10.1021/acsomega.9b02164
ACS Omega XXXX, XXX, XXX–XXX

Table 7. Kinematic Viscosity Obtained for the Filtered Brine Mixtures at Different Temperatures by Means of an Ostwald Viscometer

filtered brine mixture	kinematic viscosity (m^2/s)			
	16 °C	20 °C	25 °C	30 °C
F	1.93×10^{-6}	1.67×10^{-6}	1.48×10^{-6}	1.33×10^{-6}
G	1.84×10^{-6}	1.65×10^{-6}	1.47×10^{-6}	1.31×10^{-6}
H	1.58×10^{-6}	1.38×10^{-6}	1.24×10^{-6}	1.09×10^{-6}

Absolute Roughness of the Pipe. The absolute roughness was obtained using the relationship of Swamee and Jain[21] and the results from the clear water tests, resulting in a value for each Reynolds number. Using this analysis, a mean absolute roughness value of 0.033 mm was obtained, with a ±40% error for a 95% confidence interval and a 0.998 correlation (R^2). This value is higher than usual in smooth plastic tubes (0.0015 mm, according to Lencastre[19]), but the values of absolute roughness may present great variations due to any inner obstacle of the tube (e.g., an imperfect joint) or the aging of the material due to its contact with the brine used during the experimental campaign.

Analysis of Darcy–Weisbach Friction Factor in EF. Table 5 shows the hydraulic gradients, that is to say the linear losses per unit length, for each test and loop section, and the friction coefficients associated with each. It also shows the average hydraulic gradients for calculation of the corresponding friction coefficient. The same table shows the Reynolds number associated with each test. To calculate the number, it is necessary to know the viscosity of the tested mixtures since the brine flow is in the transition zone. The procedure for determining this physical parameter is detailed later.

The Reynolds numbers during the tests using clear water, which were the ones used to estimate the local head losses in the EF, ranged from 5.8×10^4 to 1.6×10^5.

The resulting friction coefficient is plotted in Figure 7 over the Moody diagram. The results are similar to those obtained for water, as they are also close to the curve associated with smooth pipes. As explained later, the sensitivity of the calculated friction coefficient is high; therefore, its precision is small and prevents determination of the exact results in Moody's diagram. Nevertheless, the tendency of the results to those obtained for clear water can be emphasized, albeit showing a greater dispersion in this case. The three points that differ more from the smooth turbulence line (two in relation to brine E mixture and one to brine A) correspond to the tests with the lowest flow rate. This makes sense because the sensitivity analysis explained later shows that the error associated with the calculation of the friction coefficient increases when the flow rate decreases.

Viscosity of the Tested Brine Mixtures. Figure 8 shows the curves fitted to each one of the studied brine mixtures, and Tables 6 and 7 summarize the kinematic viscosity values obtained.

In all five regressions, the experimental values for the two lower flow velocities are not over the fitted curve, which agrees with the conclusions of the sensitivity analysis of the friction factor estimation, as discussed later; the lower the flow rate, the higher the error related to the calculations. Even so, the values of R^2 in all cases are greater than 0.98 so that the fit of the regression curves with the data is high.

Figure 9 and Tables 6 and 7 present the different values of kinematic viscosity of the brine mixtures at 25 °C, for the different salt concentrations that were determined. It can be observed that although NaCl constitutes 92% of the salt, the viscosity does not correspond to that of a pure solution of this salt. The theoretical kinematic viscosities of water and the pure dilutions of $MgCl_2$,[6] KCl,[5] and NaCl,[4] for different densities but at the same temperature, are also represented in the same Figure 9.

As already presented in Table 3, the salt used in the laboratory consists of these three salts, in addition to $CaSO_4$ and a small insoluble part. The kinematic viscosities resulting from the calculations carried out follow a clear trend, that although NaCl constitutes 92% of the salt, the curve traced by the pure solution of this salt does not correspond to this

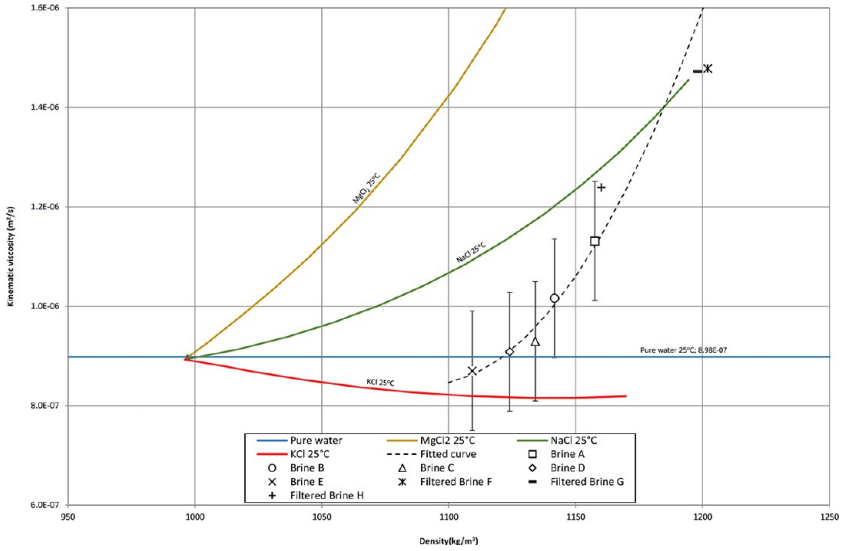

Figure 9. Experimental values of kinematic viscosity at 25 °C of the tested brine mixtures, depending on their density, and comparison of the theoretical kinematic viscosity of pure water (blue straight line) to those of pure solutions of $MgCl_2$ (brown line), NaCl (green line), and KCl (red line), all at 25 °C.

DOI: 10.1021/acsomega.9b02164
ACS Omega XXXX, XXX, XXX−XXX

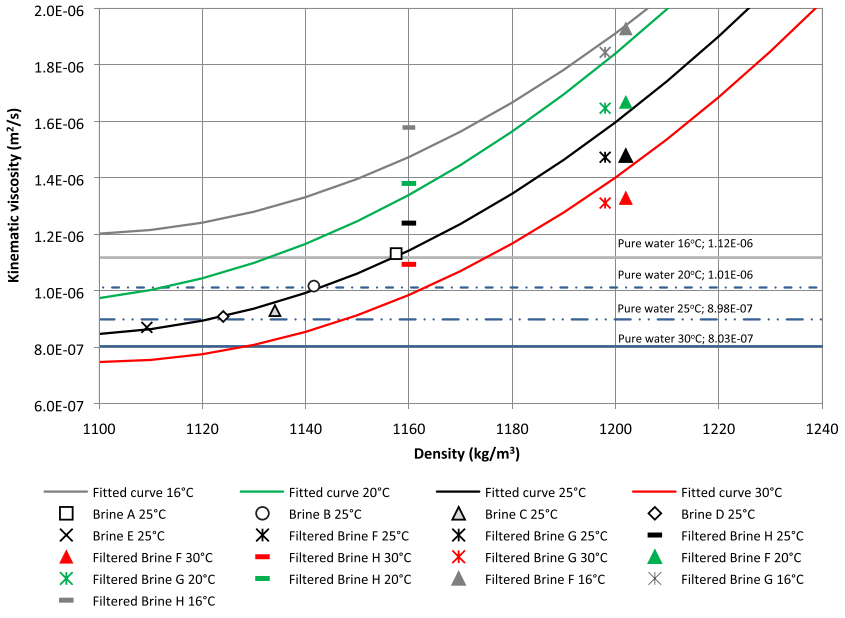

Figure 10. Experimental values of kinematic viscosity at 16, 20, 25, and 30 °C of the tested slurry mixtures and comparison with theoretical kinematic viscosity of pure water at these temperatures.

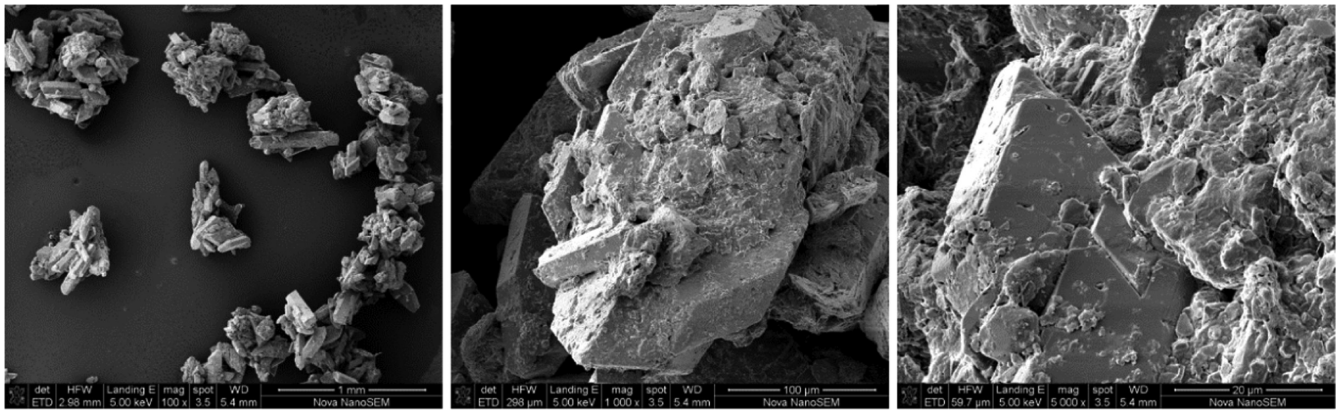

Figure 11. Images of laser microscopy of the tested sediment sample, ordered from minor (left) to major (right) magnification.

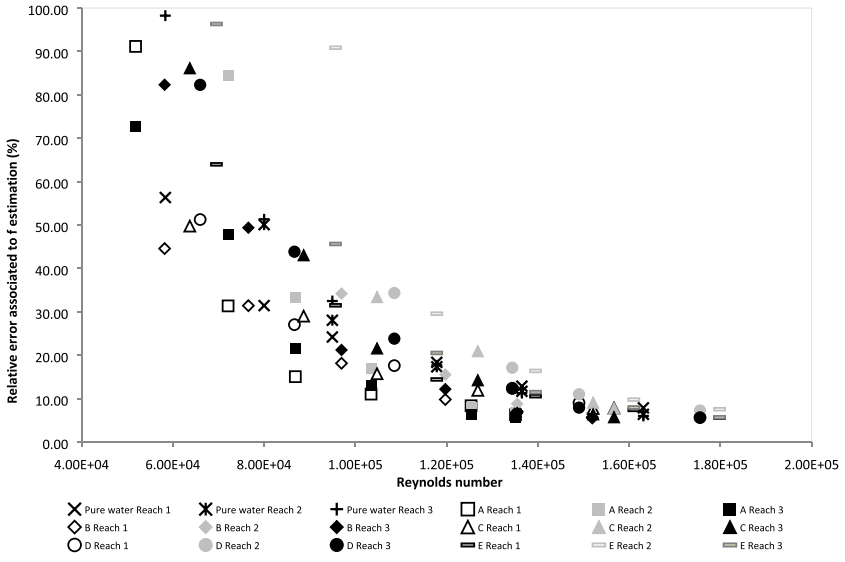

Figure 12. Accuracy of friction head losses obtained for each mixture in each section of the EF.

DOI: 10.1021/acsomega.9b02164
ACS Omega XXXX, XXX, XXX−XXX

situation. The lack of data for densities ranging from 1000 to 1100 kg/m^3 does not allow knowing the behavior of the kinematic viscosity of the brine studied in this interval, although it is below the value of the kinematic viscosity of water, following the curve pattern of the KCl solution until it reaches a density of approximately 1124 kg/m^3 (brine D). From this point, the viscosity increases rapidly as more salt is added to the mixture at a much higher rate than in the case of sodium chloride solution.

On the other hand, the filtered mixtures follow a trend closer to that corresponding to this solution. The viscosity of the filtered brines F, G, and H (eliminating solid insoluble particles) was measured by an Ostwald viscometer. A regression curve was fitted to the kinematic viscosity values of the nonfiltered mixtures at 25 °C, depending on their density, and had been subsequently adapted to the rest of the temperatures (Figure 10) to obtain a relationship among kinematic viscosity, density, and temperature.

DISCUSSION

For discussion of the results, we begin by referring to a microscopic analysis of the tested brines. This analysis points out the composition of the tested fluid, as already presented previously. Second, a sensitivity analysis of the Darcy–Weisbach friction factor is performed to characterize the accuracy of the results shown above. Next, the influence of previously obtained absolute roughness on the values of viscosity is analyzed. This analysis leads, finally, to featuring the resistance to flow of the tested brines by means of the introduction of the dimensionless pressure coefficient from the tests carried out.

Table 8. Kinematic Viscosity Deviation Obtained for the Brine Mixtures after ±40% Deviation in Absolute Roughness (k)

brine mixture	density (kg/m^3)	viscosity deviation for a 40% reduction of k (%)	viscosity deviation for a 40% increase of k (%)
A	1157.5	2.65	−2.56
B	1141.6	2.85	−2.93
C	1134.1	3.06	−3.06
D	1124.1	3.23	−3.21
E	1109.3	3.33	−3.33

Microscopic Analysis of the Tested Brine. Figure 11 shows three images obtained through laser microscopy of the solid sample deposited at stagnation points observed in Figure 3. Two kind of particles can be observed in the insoluble portion of the brine flow: the bigger sized particles with clear geometric shapes, while the rest are aggregated to the first and are amorphous. The crystalline shaped particles correspond to salt precipitates, which would have been formed during the drying process of the sediment sample. On the other hand, the amorphous aggregates correspond to the insoluble fine particles. A similar image is shown in Freyer and Voigt,[22] corresponding to calcium sulfate crystals, while in de Oliveira et al.[23] and Guo et al.,[24] cubic shapes of sodium chloride and potassium chloride crystals are presented, respectively. Therefore, it can be concluded that the analyzed sample is composed of crystals of $CaSO_4$ and insoluble particles aggregated to them.

The images also revealed the presence of salt crystals among the collected sediments for the mixtures above the limit of saturation of $CaSO_4$ (according to Bock[25]). This means that precipitation of $CaSO_4$ occurred, but no aggregates were formed on the walls of the pipe.

Sensitivity Analysis of the Darcy–Weisbach Friction Factor. Analysis of the accuracy of the Darcy–Weisbach friction factor shows that it depends on the hydraulic grade, the internal diameter and the length of the pipe, and the average flow velocity. Regarding the flow velocity, its accuracy was estimated by means of the standard deviation obtained from each test. Its estimated error ranges from 2.8% for high velocities (around 1.6 m/s) to 4.3% for the lowest (0.6 m/s). On the other hand, for the internal diameter and the length of the pipe, the error is constant and only depends on the accuracy of measurement, being ±0.1 and ±5 mm, respectively. Finally, the accuracy of the hydraulic grade is estimated applying a Monte Carlo simulation (1000 iterations) assuming a uniform probability for the errors of the variables involved in the energy balance. The error associated with the potential energy per unit of length (height of controlled cross

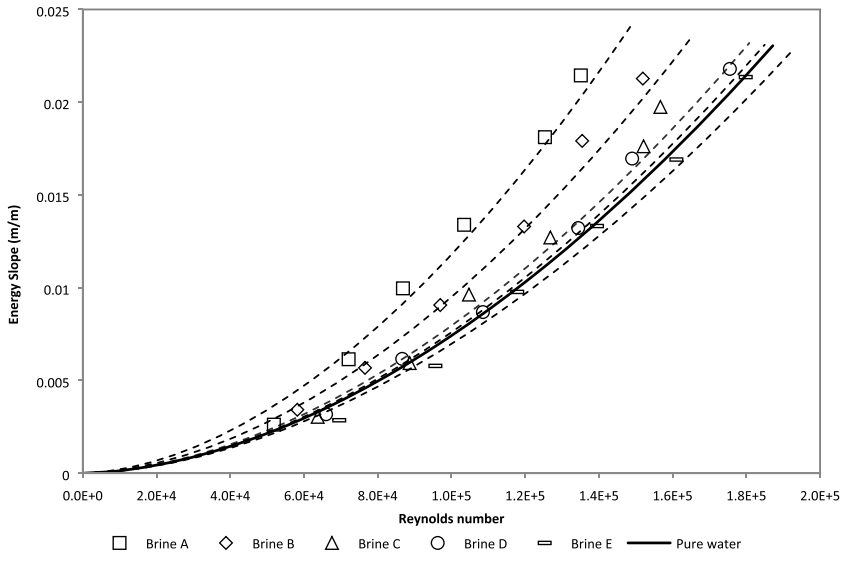

Figure 13. Energy grade from experimental data for each brine mixture.

DOI: 10.1021/acsomega.9b02164
ACS Omega XXXX, XXX, XXX−XXX

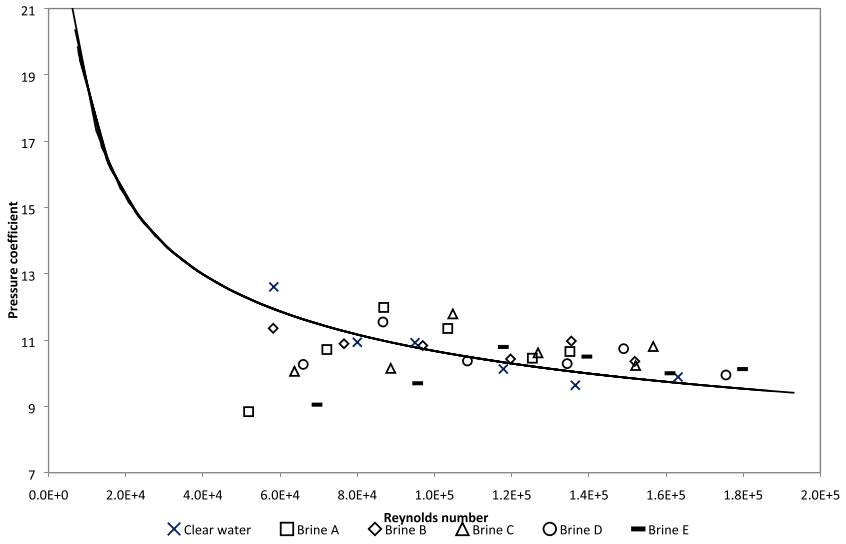

Figure 14. Estimated pressure coefficients from experimental data for each brine mixture.

sections) was assumed to be ±1 mm. On the other hand, the error of the pressure energy per unit of weight is estimated by the standard deviation of the different tests in the laboratory. The variation coefficient of each recorded time series varies depending on the sensor and the Reynolds number, and it ranges from 1.3% (sensor P4 and maximum flow rate) to 5.6% (sensor P1 and minimum flow rate).

The propagation of all of these errors on the Darcy–Weisbach friction factor, carried out by another simulation of Monte Carlo, is shown in Figure 12. As in the previous case, accuracy in the tests with lower flow velocities worsens exponentially. However, for flow velocities greater than 1 m/s, the accuracy of the Darcy–Weisbach friction factor is less than 35%.

Influence of Absolute Roughness on Viscosity. Calculation of the viscosity of brine mixtures was preceded by the calibration of the experimental loop to obtain the value of the absolute roughness of the pipe. For this purpose, as explained above, the absolute roughness k was obtained with an associated error of ±40% (for a 95% confidence interval). To know the influence of this possible error on the calculation of the viscosity of the mixtures, the process of obtaining the viscosity was repeated, imposing a variation in k within that interval of error. Table 8 shows the kinematic viscosity deviation obtained for the brine mixtures after ±40% deviation in absolute roughness value. It can be appreciated that the influence of the absolute roughness on viscosity is small, considering that a deviation of ±40% has been considered. A change in absolute roughness causes a lower variation in the values of viscosity obtained than the errors associated with the regressions carried out for calculation of viscosity (Table 6).

On the other hand, as already evident from the sensitivity analysis for the friction factor, the deviation in the results, caused by any error of calculation of the absolute roughness, is in this case higher for lower densities.

Resistance to Flow. The energy grade was obtained for each brine mixture and different Reynolds number by means of the recorded pressure values during the different tests. To illustrate the influence of increasing the total solid concentration on the flow resistance for different mixtures, the results are presented together in Figure 13. Logically, mixtures with a higher concentration of solids, and therefore higher density, have higher linear head losses and the difference with other mixtures is accentuated for higher Reynolds numbers, as viscosity becomes more important.

On the other hand, Figure 14 shows the average of all of the recorded experimental data and the curves that were fitted to determine the viscosity (in the case of brine mixtures) or absolute roughness (in the case of clear water). The curves represent the pressure coefficient (C_p) on the vertical axis and the Reynolds number on the horizontal axis

$$C_p = \frac{\frac{\Delta P}{\gamma}}{\frac{v^2}{2g}} \tag{2}$$

where $\frac{\Delta P}{\gamma}$ is the manometric increment per unit of weight in a controlled reach and $\frac{v^2}{2g}$ is the kinetic energy per unit of weight in that reach.

The presented data no longer depends on the density of the mixture or its viscosity, and for that reason, all of the data are fitted to one single curve. Anyway, it can be appreciated that, for low Reynolds numbers, brines A, C, and E show a lower fitting to the curve.

CONCLUSIONS

An experimental method to estimate the viscosity of a brine is presented. For that purpose, an experimental facility consisting of a 70 m-long PVC pipeline loop (Figure 2) was designed. Brine mixtures with solid concentrations ranging from 187 to 331 kg/m^3 were tested. The density and solid concentration of the tested brines are described in Table 1. The values of kinematic viscosity of the brine mixtures, generated at 16, 20, 25, and 30 °C for different salt concentrations, were obtained. At the same time, the viscosities of different filtered mixtures (eliminating insoluble solid particles) were measured using an Ostwald viscometer. All of the results are plotted in Figures 9 and 10 and summarized in Tables 6 and 7.

It can be observed that although NaCl constitutes 92% of the brine, the viscosity curve of the brine does not correspond to that of a pure solution of this salt. The lack of data in the range of densities from 1000 to 1100 kg/m^3 prevented knowing the behavior of the kinematic viscosity curve for this

DOI: 10.1021/acsomega.9b02164
ACS Omega XXXX, XXX, XXX−XXX

interval. For densities greater than 1124 kg/m^3, viscosity increases rapidly as more salt is added to the mixture and at a much higher rate than in the case of sodium chloride pure solution (Figure 9).

On the other hand, the results from filtered mixtures show that these follow a very similar trend to those corresponding to the nonfiltered solutions (Figure 10). A relationship among kinematic viscosity, density, and temperature was obtained by means of a regression curve fitted to the kinematic viscosity of the nonfiltered mixtures at 25 °C, depending on their density, and subsequently adapting it for the rest of the temperatures.

During the tests carried out in the experimental facility manufactured with PVC pipes, no precipitation of salts was observed inside the pipe, even when circulating a brine mixture close to the saturation limit. In spite of this, the images obtained by means of microscopy showed the presence of salt crystals among the collected sediments and it was observed that three of the mixtures generated were above the limit of saturation of $CaSO_4$ (according to Bock[25]). It seems clear, therefore, that precipitation of $CaSO_4$ occurred but did not affect the hydraulic operation of the circuit since no aggregates were formed on the walls of the pipe.

AUTHOR INFORMATION

Corresponding Author

*E-mail: marti.sanchez@upc.edu.

ORCID

Martí Sánchez-Juny: 0000-0003-2877-7711

Author Contributions

The manuscript was written through contributions of all of the authors. All authors have approved the final version of the manuscript.

Funding

Grant number 2014 DI 0070 of Industrial Doctorate Programme of Generalitat de Catalunya.

Notes

The authors declare no competing financial interest.

ACKNOWLEDGMENTS

The authors wish to thank the Agència de Gestió d'Ajuts Universitaris i de Recerca (AGAUR) of the Catalan Government for the grant number 2014 DI 0070 of the Industrial Doctorate Programme. The authors would also like to thank the company *Aigües de Barcelona* for their technical and economic support during the project's execution.

ABBREVIATIONS

EF,experimental facility; HDPE,high-density polyethylene; PVC,poly(vinyl chloride); RTD,resistance temperature detector; UPC,Universitat Politècnica de Catalunya

REFERENCES

(1) Applebey, M. P. CCXI. - The Viscosity of Salt Solutions. *J. Chem. Soc. Trans.* **1910**, *97*, 2000−2025.

(2) Dajnov, V. N. *Petróleo y Gas En Las Rocas: Métodos Geofísicos Para Determinar Sus Propiedades Colectoras y de Saturación*. Editorial Reverté: Barcelona, 1982; pp 422.

(3) *International Union of Pure and Applied Chemistry, I. Solubility Data Series - Alkali Metal and Ammonium Chlorides in Water and Heavy Water (Binary Systems)*Cohen-Adad, R., Lorimer, J. W., Eds.; Pergamon Press: Oxford, UK, 1991; pp 562.

(4) Kestin, J.; Khalifa, H. E.; Correia, R. J. Tables of the Dynamic and Kinematic Viscosity of Aqueous NaCl Solutions in the Temperature Range 20−150 °C and the Pressure Range 0.1−35 MPa. *J. Phys. Chem. Ref. Data* **1981**, *10*, 71−87.

(5) Gonçalves, F. A.; Kestin, J. The Viscosity of NaCl and KCl Solutions in the Range 25−50 °C. *Ber. Bundesforschungsanst. Phys. Chem.* **1977**, *81*, 1156−1161.

(6) Phang, S.; Stokes, R. H. Density, Viscosity, Conductance, and Transference Number of Concentrated Aqueous Magnesium Chloride at 25 °C. *J. Solution Chem.* **1980**, *9*, 497−505.

(7) Zhang, H. L.; Han, S. J. Viscosity and Density of Water + Sodium Chloride + Potassium Chloride Solutions at 298.15 K. *J. Chem. Eng. Data* **1996**, *41*, 516−520.

(8) Qiblawey, H. A.; Abu-Jdayil, B. Viscosity and Density of the Ternary Solution of Magnesium Chloride + Sodium Chloride + Water from (298.15 to 318.15) K. *J. Chem. Eng. Data* **2010**, *55*, 3322−3326.

(9) Gillies, R. G.; Shook, C. A.; Wilson, K. C. An Improved Two Layer Model for Horizontal Slurry Pipeline Flow. *Can. J. Chem. Eng.* **1991**, *69*, 173−178.

(10) Einstein, A. Eine Neue Bestimmung Der Moleküldimensionen. *Ann. Phys.* **1906**, *324*, 289−306.

(11) Kunitz, M. An Empirical Formula for the Relation between Viscosity of Solution and Volume of Solute. *J. Gen. Physiol.* **1926**, *9*, 715−725.

(12) Rutgers, I. R. Relative Viscosity and Concentration. *Rheol. Acta* **1962**, *2*, 305−348.

(13) Chong, J. S.; Christiansen, E. B.; Baer, A. D. Rheology of Concentrated Suspensions. *J. Appl. Polym. Sci.* **1971**, *15*, 2007.

(14) Konijn, B. J.; Sanderink, O. B. J.; Kruyt, N. P. Experimental Study of the Viscosity of Suspensions: Effect of Solid Fraction, Particle Size and Suspending Liquid. *Powder Technol.* **2014**, *266*, 61−69.

(15) Aigües de Barcelona. Estudio de Laboratorio Sobre La Precipitación de La Salmuera a La Salida de La Cavidad de Balsareny y En Su Recorrido a Lo Largo Del Colector de Salmueras Del Llobregat; Internal Report. Barcelona, 2011; pp 31.

(16) Museu de la Ciència i la Tècnica de Catalunya. Potassa a Súria, 100 Anys; Barcelona, 2014. http://www.spcn.cat/sites/all/files/expo_potassa_a_suria_100_anys_dossier_de_premsa.pdf (last accessed Sept 26th, 2019).

(17) Department of Geology UAB. Geozona 217 Cardona - Muntanya de La Sal; Barcelona. 2000. http://mediambient.gencat.cat/web/.content/home/ambits_dactuacio/patrimoni_natural/sistemes_dinformacio/inventari_despais_dinteres_geologic/consulta_de_les_fitxes_descriptives_dels_eig/documentos/217_descrip.pdf (last accessed Sept 26th, 2019).

(18) España Maraver, F. Aprovechamiento de Escombreras Salinas Como Materia Prima Para La Producción de Cloro-Sosa y Recuperación Del Terreno, *III Congreso Internacional de Geologia y Mineria Ambiental para el Ordenamiento Territorial y el Desarrollo*, Cardona, 2013; pp 67−68.

(19) Lencastre, A. *Manual de Ingeniería Hidráulica*, Spanish version; Universidad Pública de Navarra: 1998; pp 660.

(20) Nikuradse, J. *Strömungsgesetze in Rauhen Rohren: Mit 13 Zahlentafeln*; Forschungsheft: Verein Deutscher Ingenieure: VDI-Verlag, 1933.

(21) Swamee, P. K.; Jain, A. K. Explicit Equations for Pipe-Flow Problems. *J. Hydraul. Div.* **1976**, *102*, 657−664.

(22) Freyer, D.; Voigt, W. Crystallization and Phase Stability of CaSO4 and CaSO4-Based Salts. *Monatsh. Chem.* **2003**, *134*, 693−719.

(23) de Oliveira, J. B.; Pereira, C. S.; Gonçalves, I. A.; Vitoriano, J. O.; Junior, C. A. Sodium Chloride Crystallization by Electric Discharge in Brine. *Mater. Res.* **2017**, DOI: 10.1590/1980-5373-mr-2017-0108.

(24) Guo, X.; Yuan, J.; Ji, Z.; Su, M. Influences of Additives on the Crystal Habit of Potassium Chloride. *Front. Chem. Eng. China* **2010**, *4*, 78−81.

DOI: 10.1021/acsomega.9b02164
ACS Omega XXXX, XXX, XXX−XXX

(25) Bock, E. On the Solubility of Anhydrous Calcium Sulphate and of Gypsum in Concentrated Solutions of Sodium Chloride at 25 °c, 30 °c, 40 °c, and 50 °c. *Can. J. Chem.* **1961**, *39*, 1746−1751.

DOI: 10.1021/acsomega.9b02164
ACS Omega XXXX, XXX, XXX−XXX